

Document downloaded from:

<http://hdl.handle.net/10251/59021>

This paper must be cited as:

Penaranda-Foix, FL.; Janezic, MD.; Catalá Civera, JM.; Canós Marín, AJ. (2012). Full-wave analysis of dielectric-loaded cylindrical waveguides and cavities using a new four-port ring network. *IEEE Transactions on Microwave Theory and Techniques*. 60(9):2730-2740. doi:10.1109/TMTT.2012.2206048.



The final publication is available at

<http://dx.doi.org/10.1109/TMTT.2012.2206048>

Copyright Institute of Electrical and Electronics Engineers (IEEE)

Additional Information

“© 2012 IEEE. Personal use of this material is permitted. Permission from IEEE must be obtained for all other uses, in any current or future media, including reprinting/republishing this material for advertising or promotional purposes, creating new collective works, for resale or redistribution to servers or lists, or reuse of any copyrighted component of this work in other works.”

Full-Wave Analysis of Dielectric-Loaded Cylindrical Waveguides and Cavities Using a New Four-Port Ring Network

Felipe L. Penaranda-Foix, *Member, IEEE*, Michael D. Janezic, *Senior Member, IEEE*, Jose M. Catala-Civera, *Member, IEEE*, and Antoni J. Canos

Abstract—In this paper, a full-wave method for the electromagnetic analysis of dielectric-loaded cylindrical and coaxial waveguides and cavities is developed. For this purpose, a new 4-port ring network is proposed, and the mode-matching method is applied to calculate the Generalized Admittance Matrix (GAM) of this new structure. A number of analyses on dielectric-loaded waveguide structures and cavities have been conducted in order to validate and to assess the accuracy of the new approach. The results have been compared with theoretical values, numerical modeling from the literature, and data from commercial electromagnetic simulators. The method has been also applied to the accurate determination of dielectric properties, and we provide an example of these measurements as another way to validate this new method.

Index Terms—Electromagnetic modeling, dielectric resonator, microwave filter, mode-matching, circuit analysis, dielectric-loaded waveguides, dielectric measurements.

I. INTRODUCTION

Dielectric-loaded waveguides and cavities are increasingly being employed in passive devices, such as microwave filters or dielectric resonators, that are integrated into satellite and mobile communications systems because of their small size, low loss, and temperature stability [1]. Dielectric materials also have many important functions in the microelectronics industry. For example, new packaging technologies require substrates with low permittivity. High-permittivity materials are used to reduce the dimensions of circuits at lower frequencies. Other important new areas of applications include microwave heating [2] and sensors [3-5].

This broad range of microwave applications demands a detailed knowledge of the dielectric properties of materials, including solids, liquids, emulsions and powders [6-10]. As electrical components are miniaturized, the need for well-characterized dielectric measurements on materials increases

[11, 12]. Dielectric properties measurement strategies include waveguide cells (in reflection or/and transmission), resonators and free-space methods [13-16]. Dielectric-loaded cylindrical waveguides and cavities can provide new and accurate dielectric measurement procedures to be applied under these methodologies [17-20].

As a consequence, the study of dielectric inhomogeneities in waveguides and cavities has been a main task of microwave researchers over the last decades. The technical literature offers a large number of papers about the numerical solutions of the eigenmodes and eigenvectors of canonical metallic cavities loaded with dielectric resonators. The finite-element method (FEM) [21] and finite-difference time-domain (FDTD) [22] procedures have been primarily employed to solve this problem. The need to employ refined 3D meshes, and the frequency dependence of calculations, make these methods very demanding in terms of computation time and memory resources.

To overcome these limitations, the Mode-Matching (MM) method [23-26] has emerged as an efficient and accurate technique to solve waveguide discontinuities and cavities. The boundary integral-resonant-mode expansion (BI-RME) technique [27, 28] has also been efficiently applied to the analysis of dielectric-loaded cavities of rectangular shape. For complex or large size waveguides or cavities, however, the MM method may suffer from convergence problems, and it has been combined with other analytical techniques [29-32]. Circuit analysis and segmentation have also proved to be powerful tools for analyzing complex dielectric-filled structures [33-35]. The generalized circuit analysis is a method for solving electromagnetic problems that consists of the segmentation of the whole geometry of the microwave structure into simpler elements, which then can be solved in an easier way [25, 36-41]. Once the simpler structures have been solved separately, they can be joined or combined through the use of the Generalized Admittance Matrix (GAM) in order to give the complete solution of the complex structure.

In this paper, the calculation of the GAM matrix of a new 4-port dielectric ring network is proposed. The term 4-port does not refer to the terminals of the entire structure that is being analyzed. As shown in Figure 2, this 4-port ring

Manuscript received December, 2011.

Felipe L. Penaranda-Foix, Jose M. Catala-Civera and Antoni J. Canos are with Instituto ITACA, Universidad Polit cnica de Valencia, Camino de Vera, s/n, 46022-Valencia, Spain (Felipe L. Penaranda-Foix, the corresponding author, phone: +34-96 387 9711; e-mail: fpenaran@dcop.upv.es).

Michael D. Janezic is with the National Institute of Standards and Technology-NIST 325 Broadway, MS 818.01; Boulder, CO 80305 USA.

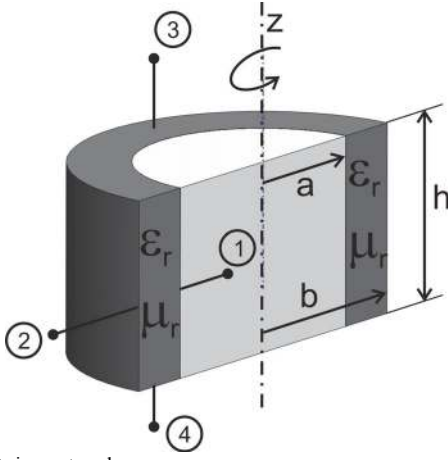


Fig. 1. 4-port ring network.

network is only one of the elements, used in conjunction with other circuit elements, to model the larger structure. A 4-port dielectric ring network is necessary because of the multiple dielectric layers that can occur in both the radial (ports 1 and 2) and axial (ports 3 and 4) directions, as shown in Figure 1. The GAM will be computed using the MM method, where the field in each port is approximated by a series expansion of basis functions. The set of basis functions has been chosen so that one can solve the resulting integrals analytically, without having to employ numerical methods. The combination of this new network with other circuit elements, such as cylindrical or coaxial waveguides, will allow an efficient and accurate tool to the full-wave solution of the scattering matrix or the resonant frequencies of dielectric-loaded cylindrical structures. Dielectric resonator filters and dielectric-filled re-entrant coaxial waveguides and cavities can be solved straightforwardly with the use of the developed full-wave analysis method. Moreover, the use of microwave cavities partially filled with two dielectrics shows a clear application of the method for measuring the dielectric properties of materials [42, 43].

The validity of the proposed 4-port dielectric ring network is examined by modeling different well-known cylindrical transmission-line and cavity structures and then comparing the results with those included in the technical literature as well as with those given by other numerical techniques. Measurements of some microwave devices are also included for validation purposes.

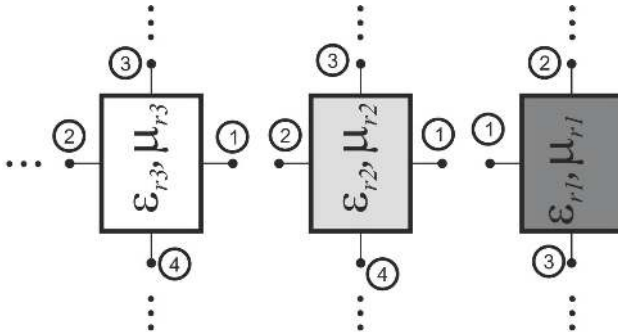


Fig. 2. Example of several 4-port and 3-port interconnection networks to model a multilayer structure.

II. THEORY

Figure 1 shows the proposed 4-port network to be analyzed. It consists of a toroid with inner radius a , outer radius b , and height h , with permittivity ϵ_r ($\epsilon_r = \epsilon' - j\epsilon''$) and permeability μ_r ($\mu_r = \mu' - j\mu''$). The four ports are defined as follows: port 1 at $r=a$, $0 \leq z \leq h$, port 2 at $r=b$, $0 \leq z \leq h$, port 3 at $a \leq r \leq b$, $z=h$ and port 4 at $a \leq r \leq b$, $z=0$.

The 4-port network can be combined with other networks by circuit analysis to model more complex structures. As an example, Figure 2 shows how this 4-port network can be interconnected to other 3-port networks [44] to model a multilayer structure composed of several dielectric materials. The proposed circuit analysis enables the calculation of either the scattering parameters, in the case of a transmission-line structure, or the resonant frequencies for cavities or resonators.

The GAM of a 4-port network is defined by the general expression (1):

$$\mathbf{Y} = \begin{pmatrix} \mathbf{Y}_{11} & \mathbf{Y}_{12} & \mathbf{Y}_{13} & \mathbf{Y}_{14} \\ \mathbf{Y}_{21} & \mathbf{Y}_{22} & \mathbf{Y}_{23} & \mathbf{Y}_{24} \\ \mathbf{Y}_{31} & \mathbf{Y}_{32} & \mathbf{Y}_{33} & \mathbf{Y}_{34} \\ \mathbf{Y}_{41} & \mathbf{Y}_{42} & \mathbf{Y}_{43} & \mathbf{Y}_{44} \end{pmatrix} \quad (1)$$

It is important to note that each element in the GAM is a matrix that relates the modes in one port to the modes in remaining ports [26, 45, 46].

In general, the elements in (1) represent TEM, TM or TE modes. However, the analysis described here is restricted to the TM modes with symmetry of revolution (TM_{0n}). Therefore, because of the particular geometry of the structures defined in Fig. 1, only TEM and TM modes are taken into account in the model. This restriction is strictly due to the type of the structures we are interested in, and it does not represent a loss of generality of the GAM technique. The procedure is in fact similar to the one followed in [47], where only TE_{0np} modes were employed to analyze the split post dielectric resonator.

With these assumptions, we define the components of the electromagnetic fields in the inner region ($a \leq r \leq b$) as [48]:

$$\begin{aligned} E_z &= \sum_{n=0}^{\infty} f_{0n}(r) (a_n e^{-\gamma_n z} + b_n e^{+\gamma_n z}) \\ E_r &= \sum_{n=0}^{\infty} \frac{-\gamma_n}{k_{c0n}} \cdot f'_{0n}(r) (a_n e^{-\gamma_n z} - b_n e^{+\gamma_n z}) \\ H_\phi &= \sum_{n=0}^{\infty} \frac{-j\omega\epsilon_0\epsilon_r}{k_{c0n}} f'_{0n}(r) (a_n e^{-\gamma_n z} + b_n e^{+\gamma_n z}) \end{aligned} \quad (2)$$

where $f_{0n}(r)$ and $f'_{0n}(r)$ are:

$$f_{0n}(r) = \begin{cases} 0, & n = 0 \\ J_0(k_{c0n}r) + \Gamma_n Y_0(k_{c0n}r), & n > 0 \end{cases} \quad (3)$$

$$f'_{0n}(r) = \begin{cases} -1/(r\gamma_0), & n = 0 \\ -J_1(k_{c0n}r) - \Gamma_n Y_1(k_{c0n}r), & n > 0 \end{cases}$$

In (3), the values of k_{c0n} (cut-off wave number) depend on the boundary conditions and the value of Γ_n . The mode $n=0$ corresponds to the TEM mode, where $k_{c0n}|_{n=0} = 0$. However, in order to define (2) and (3) with more generality, and to include TEM mode, the criteria of $k_{c00}=1$ is adopted hereinafter.

The propagation constant γ_n and the cut-off wave number k_{c0n} are related as follows:

$$k_{c0n}^2 = k^2 + \gamma_n^2 \quad (4)$$

where k is the free-space wave number $k = \omega\sqrt{\epsilon\mu}$.

The functions $J_n(\cdot)$ and $Y_n(\cdot)$ in (3) are, respectively, the Bessel functions of the first and second kind with order n (0 or 1), and Γ_n is a coefficient that depends on the boundary conditions.

The next subsection describes the calculation of the set of parameters \mathbf{Y}_{i1} , ($i=1,2,3,4$) of (1).

A. Parameters \mathbf{Y}_{i1}

To calculate the \mathbf{Y}_{i1} parameters, electric wall conditions are imposed on ports 2, 3 and 4, therefore, fields in (2) become:

$$\begin{cases} E_r|_{z=0} = 0 \\ E_r|_{z=h} = 0 \\ E_z|_{r=b} = 0 \end{cases} \Rightarrow \begin{cases} a_n = b_n \\ \gamma_n = j\frac{n\pi}{h} \\ \Gamma_n = -J_0(k_{c0n}b)/Y_0(k_{c0n}b) \end{cases} \quad (5)$$

By substituting the above relations in (2), the electromagnetic fields in the inner region are:

$$E_z = \sum_{n=0}^{\infty} 2a_n f_{0n}(r) \cosh(\gamma_n z) \quad (6)$$

$$E_r = \sum_{n=0}^{\infty} 2a_n \frac{\gamma_n}{k_{c0n}} f'_{0n}(r) \sinh(\gamma_n z)$$

$$H_\phi = \sum_{n=0}^{\infty} 2a_n \frac{-j\omega\epsilon_0\epsilon_r}{k_{c0n}} f'_{0n}(r) \cosh(\gamma_n z)$$

Given the propagation constant γ_n , the value of the cut-off wave numbers can be calculated as:

$$k_{c0n}^2 = k^2 + \gamma_n^2 = k^2 - \left(\frac{n\pi}{h}\right)^2 \quad (7)$$

In this case, the TEM mode does not exist because of the

resulting geometry when short-circuiting ports 2, 3 and 4. However, it must be noted that when computing the \mathbf{Y}_{i3} and \mathbf{Y}_{i4} parameters, the TEM mode does exist and thus it must be included.

The incident electric field at port 1 is:

$$E_z = \sum_{m=0}^{\infty} \alpha_m \sin\left(2\pi m \frac{z}{h}\right) + \beta_m \cos\left(2\pi m \frac{z}{h}\right) \quad (8)$$

where we assume a Fourier series expansion, based on trigonometric basis functions, for this port.

Next, we equate (8) and the E_z field in (6) at $r=a$, and calculate the amplitudes a_n using the orthogonal properties of the trigonometric functions. We then obtain :

$$a_n = \frac{\chi_n}{hf_{0n}(a)} \sum_{m=0}^{\infty} \alpha_m \cdot I_{mn}^{(s)} + \beta_m \cdot I_{mn}^{(c)} \quad (9)$$

where $I_{mn}^{(s)}$, $I_{mn}^{(c)}$ and χ_n are defined in Appendix, section A.

Parameter \mathbf{Y}_{11}

In (10) the magnetic field at port 1 is written as a series expansion similar to the incident electric field defined in (8):

$$H_\phi = \sum_{q=0}^{\infty} c_q \sin\left(2\pi q \frac{z}{h}\right) + d_q \cos\left(2\pi q \frac{z}{h}\right) \quad (10)$$

The magnetic field at port 1 and the inner magnetic field from (6) must be equal at $r=a$, which leads to the following expressions:

$$\begin{aligned} & \sum_{q=0}^{\infty} c_q \sin\left(2\pi q \frac{z}{h}\right) + d_q \cos\left(2\pi q \frac{z}{h}\right) = \\ & = \sum_{n=0}^{\infty} 2a_n \frac{-j\omega\epsilon_0\epsilon_r}{k_{c0n}} f'_{0n}(a) \cosh(\gamma_n z) \\ & \quad \downarrow \\ & c_q = \frac{2}{h} \sum_{n=0}^{\infty} 2a_n \frac{-j\omega\epsilon_0\epsilon_r}{k_{c0n}} f'_{0n}(a) I_{qn}^{(s)} \\ & d_q = \frac{2\chi_q}{h} \sum_{n=0}^{\infty} 2a_n \frac{-j\omega\epsilon_0\epsilon_r}{k_{c0n}} f'_{0n}(a) I_{qn}^{(c)} \end{aligned} \quad (11)$$

Since parameter \mathbf{Y}_{11} is defined as the relation between the electric and magnetic fields at port 1, we have:

$$\mathbf{h}_1 = \begin{pmatrix} \mathbf{c} \\ \mathbf{d} \end{pmatrix} = \mathbf{Y}_{11} \cdot \mathbf{e}_1 = \begin{pmatrix} \mathbf{Y}_{11}^{(ss)} & \mathbf{Y}_{11}^{(sc)} \\ \mathbf{Y}_{11}^{(cs)} & \mathbf{Y}_{11}^{(cc)} \end{pmatrix} \cdot \begin{pmatrix} \mathbf{a} \\ \mathbf{\beta} \end{pmatrix} \quad (12)$$

where each submatrix $\mathbf{Y}_{11}^{(xy)}$, being $(x, y) \in (s, c)$, is derived from (11) as follows:

$$Y_{11}^{(ss)}|_{qm} = \frac{2}{h} \sum_{n=0}^{\infty} \frac{-j\omega\epsilon_0\epsilon_r}{k_{c0n}} \frac{f'_{0n}(a)}{f_{0n}(a)} 2\chi_n \frac{I_{mn}^{(s)}}{h} I_{qn}^{(c)} \quad (13a)$$

$$Y_{11}^{(sc)}|_{qm} = 0 \quad (13b)$$

$$Y_{11}^{(cs)}|_{qm} = 0 \quad (13c)$$

$$Y_{11}^{(cc)}|_{qm} = \frac{2\chi_q}{h} \sum_{n=0}^{\infty} \frac{-j\omega\epsilon_0\epsilon_r}{k_{c0n}} \frac{f'_{0n}(a)}{f_{0n}(a)} 2\chi_n \frac{I_{mn}^{(c)}}{h} I_{qn}^{(c)} \quad (13d)$$

Parameter \mathbf{Y}_{2l}

The calculation of parameter \mathbf{Y}_{2l} is obtained in a similar way to the \mathbf{Y}_{1l} parameter, noting that port 2 is now placed at $r=b$.

Parameter \mathbf{Y}_{3l}

The magnetic field at port 3 is written as a series expansion of the basis functions $h_q^{(3)}(r)$:

$$H_\phi = \sum_{q=0}^{\infty} c_q h_q^{(3)}(r) = \sum_{q=0}^{\infty} c_q \omega_{1q}^{(3)}(r) N_q^{(e3)}, \quad a \leq r \leq b \quad (14)$$

where the basis functions $h_q^{(3)}(r)$ used at port 3 and at port 4 are orthogonal in the range $a \leq r \leq b$. They are a complete set of Bessel functions, which makes them suitable for structures that can be described in circular-cylindrical coordinates. The series expansion used is a generalization of the Dini series expansions [49] as they were developed in [50]. This series expansion is included in Appendix, section B (superindex ⁽³⁾ in function $\omega_{1q}^{(3)}(r)$ refers to port 3). The term $N_q^{(e3)}$ is a normalization term for the electric field [51, 52]. This term is also calculated in Appendix, section C.

By equating the magnetic field at port 3 with the inner magnetic field, defined in (6), over the region $z=h$, we get:

$$\begin{aligned} & \sum_{q=0}^{\infty} c_q \omega_{1q}^{(3)}(r) N_q^{(e3)} = \\ & = \sum_{n=0}^{\infty} 2a_n \frac{-j\omega\epsilon_0\epsilon_r}{k_{c0n}} f'_{0n}(r) \cosh(\gamma_n h) \quad (15) \\ & \quad \quad \quad \downarrow \\ c_q & = \frac{1}{B_q^{(3)} N_q^{(e3)}} \sum_{n=0}^{\infty} 2a_n \frac{-j\omega\epsilon_0\epsilon_r}{k_{c0n}} \cos(n \cdot \pi) I_{qn}^{(\omega)} \end{aligned}$$

where $N_q^{(e3)}$ has been defined in (37) and $B_q^{(3)}$ in (34) and $I_{qn}^{(\omega)}$ is defined in Appendix, section D.

Defining the parameter \mathbf{Y}_{3l} as the relation between the magnetic field at port 3 and electric field at port 1, we have:

$$\mathbf{h}_3 = \mathbf{c} = \mathbf{Y}_{3l} \cdot \mathbf{e}_1 = \begin{pmatrix} \mathbf{Y}_{3l}^{(s)} & \mathbf{Y}_{3l}^{(c)} \end{pmatrix} \cdot \begin{pmatrix} \mathbf{a} \\ \mathbf{b} \end{pmatrix} \quad (16)$$

where each submatrix $\mathbf{Y}_{3l}^{(x)}$, being $(x) \in (s, c)$ is from (15):

$$Y_{31}^{(s)}|_{qm} = \frac{1}{B_q^{(3)} N_q^{(e3)}} \quad (17a)$$

$$\cdot \sum_{n=0}^{\infty} \frac{-j\omega\epsilon_0\epsilon_r}{k_{c0n}} 2\chi_n \frac{\cos(n\pi)}{f_{0n}(a)} \frac{I_{mn}^{(s)}}{h} I_{qn}^{(\omega)}$$

$$Y_{31}^{(c)}|_{qm} = \frac{1}{B_q^{(3)} N_q^{(e3)}} \quad (17b)$$

$$\cdot \sum_{n=0}^{\infty} \frac{-j\omega\epsilon_0\epsilon_r}{k_{c0n}} 2\chi_n \frac{\cos(n\pi)}{f_{0n}(a)} \frac{I_{mn}^{(c)}}{h} I_{qn}^{(\omega)}$$

Parameter \mathbf{Y}_{4l}

The calculation of parameter \mathbf{Y}_{4l} is obtained in a similar manner to the \mathbf{Y}_{3l} parameter, but in the region $z=0$.

B. Parameters \mathbf{Y}_{i2} , \mathbf{Y}_{i3} and \mathbf{Y}_{i4}

Since the remaining parameters of columns 2, 3 and 4 of the \mathbf{Y} -matrix are calculated in a similar way to the parameters in the first column, \mathbf{Y}_{i1} , we do not include here (for the sake of space) how their expressions are determined.

C. Losses in the Electric walls

Dielectric or magnetic losses of the material in the ring circuit of Figure 1 are included in the imaginary parts of the complex permittivity and complex permeability respectively, as defined in previous paragraphs, but the conductive losses associated with the electric walls requires an additional explanation. The impedance associated with a finite conductivity electric wall can be calculated with the well-known expression [53- 55]:

$$Z_{short} \approx R_s(1+j), \quad R_s = \frac{1}{\sigma\delta} = \sqrt{\frac{\pi f \mu}{\sigma}} \quad (18)$$

The same expression can be retrieved from the computed GAM matrix. Assuming $b \rightarrow \infty$, we obtain a 1-port element where the unique GAM parameter is \mathbf{Y}_{1l} . From the second Maxwell equation, a good dielectric satisfies $\sigma/(\omega\epsilon) \ll 1$ and a good conductor satisfies $\sigma/(\omega\epsilon) \gg 1$ (see [48, 56]). Thus, for a good conductor, we can assume that the following permittivity relationship applies:

$$\epsilon = \frac{-j\sigma}{\omega} \quad (19)$$

The open space wave number k associated with this permittivity is:

$$k^2 = \omega^2 \mu \epsilon = -j\omega\mu\sigma \Rightarrow k = \frac{1+j}{\delta} \quad (20)$$

where δ is the penetration depth used in (18). Using (20) in parameter \mathbf{Y}_{1l} , we obtain the following expression:

$$\frac{f'_{0n}(a)}{f_{0n}(a)} = \frac{-J_1(k_{c0n}a) - \frac{J_0(k_{c0n}b)}{Y_0(k_{c0n}b)} Y_1(k_{c0n}a)}{J_0(k_{c0n}a) + \frac{J_0(k_{c0n}b)}{Y_0(k_{c0n}b)} Y_0(k_{c0n}a)} \Big|_{b \rightarrow \infty} \approx (21)$$

$$\approx -\frac{H_1^{(2)}(k_{c0n}a)}{H_0^{(2)}(k_{c0n}a)}$$

where the cut-off wave number k_{c0n} is (7):

$$k_{c0n}^2 = k^2 + \gamma_n^2 = \omega^2 \mu \epsilon - \left(\frac{n\pi}{h}\right)^2 = -j\omega\mu\sigma - \left(\frac{n\pi}{h}\right)^2 (22)$$

For most metals, the value of the conductivity σ is relatively high, so the expression for the wave number can be approximated by:

$$k_{c0n}^2 \approx -j\omega\mu\sigma (23)$$

Then, with respect to Y_{1l} we have:

$$Y_{1l}^{(ss)} \Big|_{qm} \approx \frac{-1}{1+j} \frac{1}{R_s} \delta(m-q) (24a)$$

$$Y_{1l}^{(sc)} \Big|_{qm} = 0 (24b)$$

$$Y_{1l}^{(cs)} \Big|_{qm} = 0 (24c)$$

$$Y_{1l}^{(cc)} \Big|_{qm} \approx \frac{-1}{1+j} \frac{1}{R_s} \delta(m-q) (24d)$$

where $\delta(\cdot)$ is the Dirac delta function. As expected, the 1-

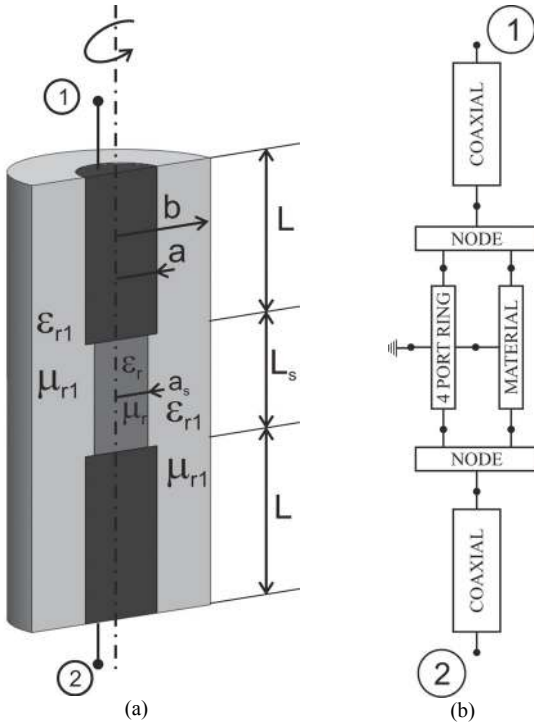


Fig. 3. Re-entrant coaxial waveguide and its circuit segmentation.

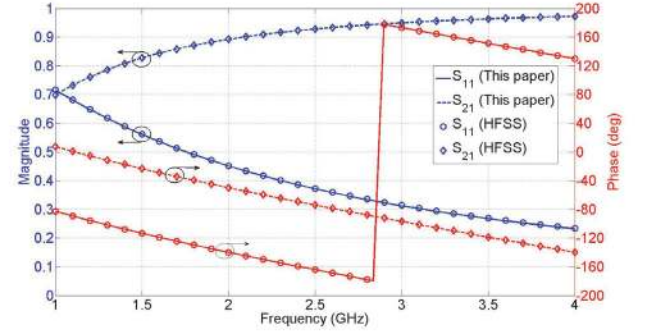


Fig. 4. Magnitude and phase of the S parameters with air gap when $a=7.25\text{mm}$, $b=24.9\text{mm}$, $a_s=10\text{mm}$, $L_s=2\text{mm}$, $L=15\text{mm}$ and $\epsilon_r=1$.

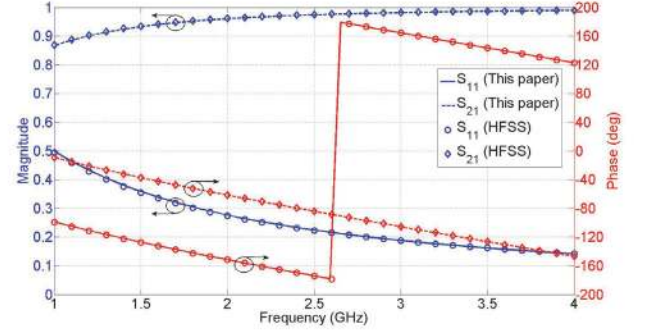


Fig. 5. Magnitude and phase of the S parameters with air gap when $a=7.25\text{mm}$, $b=24.9\text{mm}$, $a_s=10\text{mm}$, $L_s=2\text{mm}$, $L=15\text{mm}$ and $\epsilon_r=2-j*0.002$.

port network GAM for the finite conductive electric wall results in a diagonal matrix with the impedance value of (18). The sign discrepancy comes from the Poynting vector flux that in the present paper is outgoing from the network and not ingoing as usual. Applying this standard criterion, the sign of the magnetic field changes, which also changes the sign of the GAM, leading to the same value for (18).

III. NUMERICAL RESULTS AND DISCUSSION

In order to validate the accuracy of the numerical model described in the previous section, and demonstrate the usefulness of the combination of this new 4-port network with cylindrical or coaxial waveguides, modeling results of typical dielectric-loaded microwave structures are compared with analytical expressions, general-purpose FEM simulators and with results previously published in the literature. This is shown in sections III.A, III.B, III.C and III.D. Section III.E includes an example of permittivity measurements as illustrative of another application of the proposed network.

A. Coaxial waveguide loaded with a dielectric disk

Fig. 3-(a) shows a coaxial waveguide with a cylindrical dielectric sample positioned between the two inner conductors. Figure 3-(b) shows how this structure is broken down into different networks, where the proposed 4-port ring network is combined with 1-port (short-circuit), 2-port (coaxial line), and 3-port (node) networks (see [33, 44] for details of this networks).

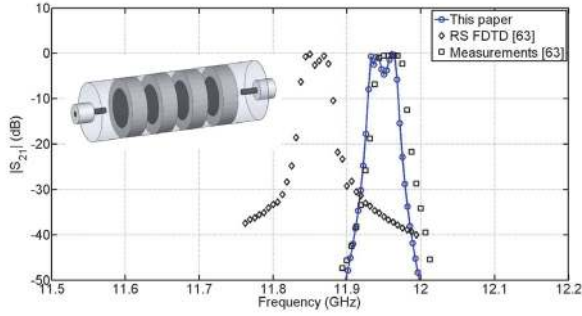


Fig. 6. 4-pole TM_{01} Dielectric Resonator Filter (see dimensions in [63]).

Figs. 4 and 5 show the magnitude and phase of the S-parameters of the 2-port structure calculated by joining the nodes and networks described in Figure 3-(b) for a dielectric disc of permittivity of air and permittivity of $\epsilon_r=2-j\cdot 0.002$, respectively. Dimensions of the geometry are given in the figure caption. Only 15 modes over 50 frequency points were required to solve the dielectric-loaded coaxial in less than 6 seconds with a PC (Intel Core i5-2320 and 6 GB RAM). The computed results (labeled MODAL) are in very good agreement with those provided by the commercial code Ansoft HFSS (labeled HFSS) also included in the Figures for comparison. Of course, the accuracy of the modeling depends on the number of modes selected to perform the calculations. The number of modes has a direct impact on the required processing time. In this, and in the rest of the simulated cases, good accuracy has been reached, when compared with references in the literature, by selecting only a few modes (i.e. 15 modes in this first example), which allows one to analyze the structures in a reasonable amount of time.

By short-circuiting (perfect electric walls are assumed in the simulation) both ends (ports 1 and 2), and imposing resonant condition [57], this structure becomes a re-entrant cavity, which is a common device for measuring the complex permittivity of dielectric materials, as described in [29, 58-62].

B. Cylindrical Dielectric Resonant (DR) Filters

The second structure considered is a 4-pole TM_{01} Dielectric Resonator (DR) filter shown in Figure 6 [63]. It consists of a set of spaced dielectric-loaded cylindrical waveguides coupled by coaxial lines. The dielectric support of the dielectric resonator has a relative permittivity of 1.031, and the rest of parameters are given in the figure caption. To solve for the S-parameters of this structure, the schematic of Figure 6 is segmented by connecting the nodes of the 4-port network to cylindrical waveguides in a similar manner to the coaxial of Figure 3.

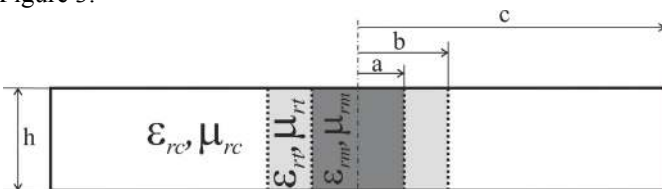


Fig. 7. Coaxially loaded cavity with container.

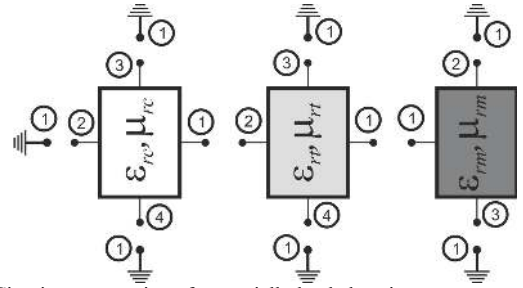


Fig. 8. Circuit segmentation of a coaxially loaded cavity.

The computed S-parameters for the 4-pole filter are shown in Figure 6. To obtain an accurate S-parameters over 150 frequency points, we included 30 modes, which resulted in a total computation time of 60 seconds using a laptop (Intel Core i5 and 6 GB RAM). The computed performance of the 4-pole filter is compared in Figure 6 with simulations and measurements of the same structure carried out in [63]. Very good agreement with measurements is observed from the figure.

C. Cylindrical cavity coaxially-loaded with two dielectric materials

The third structure to be studied with the proposed method is a cylindrical cavity coaxially-loaded with two dielectric materials that extends along the cavity height, as shown in Figure 7. This inhomogeneous cavity can be solved analytically, giving us the opportunity to compare the accuracy of the proposed model with previously-published analytical results. For this configuration, ports 1 and 2 of the 4-port network are joined with the materials in contact, whereas ports 3 and 4 are short-circuited (see Figure 8). The 3-port network of Fig. 8 is described in [44]. Short-circuits can be modeled either as perfect conductors (PEC) or conductors with a finite conductivity, as described previously in the Theory section. Resonant frequencies and quality factors have been calculated using the resonant condition [57] and the complex resonant frequency concept [56].

Table I shows the first two resonant frequencies and Q-factors corresponding to the TM_{0np} (TM_{010} and TM_{020}) modes

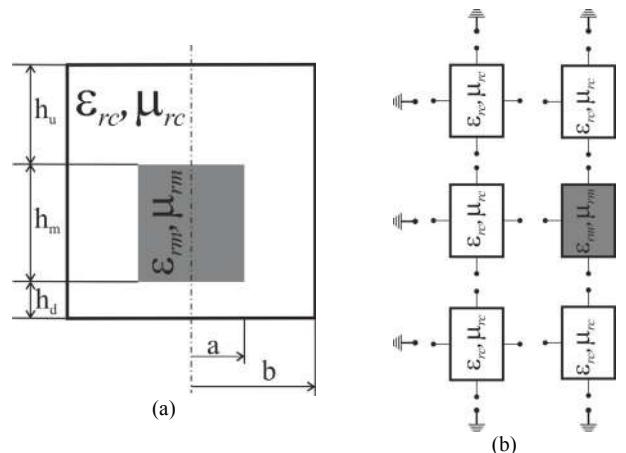


Fig. 9. Cylindrical cavity partially loaded with a dielectric disk (a) and circuit segmentation (b).

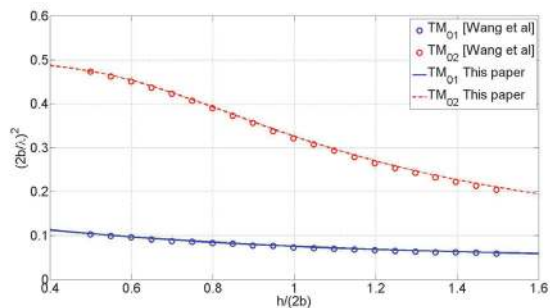


Fig. 10. Resonant frequency of the first 2 TM modes, with $a/b=0.3$, $a=20$ mm, $h_m/h=0.9$ and $\epsilon_r=36$.

of a cylindrical cavity coaxially-loaded with dielectric materials of different permittivity, and first resonant mode TM_{010} when the dielectric is inside a dielectric tube. In both cases (with and without tube), the calculated values are identical to those provided by an analytical solution of this structure [48] so that we can assess the accuracy and performance of this technique. In order to compare with the analytic solutions, the conductivity of the walls is assumed infinite ($\sigma=\infty$). In all the cases the resonant frequencies provided by the Ansoft HFSS simulations are included, and the relative errors are about 1.3% in the resonant frequencies

TABLE I
RESONANT FREQUENCY COMPARISONS
 $a=15$ mm; $b=20$ mm; $c=50$ m; $h=20$ mm

		f (GHz)	Q
MODE 1 $\epsilon_{rm}=2 \cdot (1-j \cdot 10^{-2})$ $\epsilon_{rt}=2 \cdot (1-j \cdot 10^{-2})$	Analytic	1.8736	144.536
	This paper	1.8736	144.536
	HFSS	1.8988	144.466
MODE 2 $\epsilon_{rm}=2 \cdot (1-j \cdot 10^{-2})$ $\epsilon_{rt}=2 \cdot (1-j \cdot 10^{-2})$	Analytic	4.5788	265.069
	This paper	4.5788	265.069
	HFSS	4.6409	264.948
MODE 1 $\epsilon_{rm}=5 \cdot (1-j \cdot 10^{-4})$ $\epsilon_{rt}=5 \cdot (1-j \cdot 10^{-4})$	Analytic	1.3020	11444.3
	This paper	1.3020	11444.3
	HFSS	1.3192	11442.2
MODE 2 $\epsilon_{rm}=5 \cdot (1-j \cdot 10^{-4})$ $\epsilon_{rt}=5 \cdot (1-j \cdot 10^{-4})$	Analytic	3.7356	16965.3
	This paper	3.7356	16965.3
	HFSS	3.7857	19938.0
MODE 1 $\epsilon_{rm}=5 \cdot (1-j \cdot 10^{-4})$ $\epsilon_{rt}=2 \cdot (1-j \cdot 10^{-2})$	Analytic	1.4322	698.79
	This paper	1.4322	698.79
	HFSS	1.4515	698.88

TABLE II
SIMULATIONS OF RESONANT FREQUENCIES (IN GHz)
 $\epsilon_r=35.74$; $a=0.8636$ cm; $b=1.295$ cm; $h_m=0.762$ cm; $h_u=h_d=0.381$ cm

Mode	[1]	[65]	This paper	Relative error (%) with [1] and [65] respectively
TM_{01}	4.568	4.5442	4.5410	0.60 0.07
TM_{02}	6.384	6.361	6.3732	0.17 -0.19
TM_{03}	7.323	7.254	7.2622	0.84 -0.11
TM_{04}	7.685	7.641	7.6614	0.31 -0.27
TM_{05}	9.169	9.093	9.1078	0.67 -0.16
TM_{06}	10.031	9.942	9.9827	0.48 -0.41

and 0.05% in the quality factors.

D. Cylindrical cavity partially loaded with a dielectric disk

The next structure analyzed is a cylindrical cavity partially-filled with a dielectric disk that can be located at different height (see Figure 9-a). This cavity can be split into simple circuit elements, as shown in Figure 9-b, where the 4-port ring network is connected to the other 4-port ring networks (up and down) and terminated with short-circuits [44].

Figure 10 shows the calculated resonant frequencies of the first two modes (TM_{01} and TM_{02}) as a function of the rate between the cavity height and the dielectric disk diameter when the material is placed at the bottom ($h_d=0$) and for a given value of permittivity (comb-line resonator). For comparison, the figure also reproduces the results given by [64] of the same structure, showing again very good agreement between both approaches.

The cavity loaded with the dielectric disk at the center ($h_d=h_u$), as represented in Figure 9-(a), has been extensively used in the literature to compare different methods of analysis. Therefore, we compare our results with those obtained by the orthonormal basis method [1] and with the mode-matching method of [65]. Table II presents a list with some of these results corresponding to the TM_{0n} modes. Again, we find excellent agreement between our results and those using other approaches, which confirm the validity of the developed method (the conductivity is assumed to be infinite, because no information about it is provided in the references).

In order to compute each resonant frequency, the Nelder-Mead minimization method was used [66], with an average of 180 evaluations when we included 30 modes, resulting in a computation time of 180 seconds per frequency point.

E. Dielectric measurements with cylindrical cavity partially loaded with a dielectric disk

Finally, we included an example of permittivity measurements of a dielectric disk in the cylindrical cavity depicted in Figure 9-(a), with $h_d=0$. Table III shows the measurements of the resonant frequency and Q-factor of the cylindrical cavity containing samples of ceramic materials (with high and low permittivity values) and the calculated permittivity of the samples using the circuital representation of Figure 9-(b). Resonance measurements have been carried out following the procedures described in [67]. Dimensions of cavity and samples are also given in the table, as well as the measured conductivity, which is determined through a measurement of the empty cavity.

The calculated results show very good agreement with the values provided by the material manufacturer's data sheet and with other measurements performed in a split-cylinder resonator at NIST, thereby confirming the validity of the developed approach to accurately measure the dielectric properties of materials.

IV. CONCLUSION

In this paper, the GAM of a novel 4-port cylindrical ring network has been successfully solved. The combination of the proposed ring circuit network with coaxial and cylindrical waveguides can be used to model a variety of complex structures. For instance, they have been used for solving dielectric-loaded structures widely employed as microwave devices and resonators, including those with finite conductivity walls.

This new element has been used to calculate the S-parameters, resonant frequencies and quality factor of some dielectric loaded structures with dielectric disks.

The results provided by this new element have been compared with theoretical results, as well as with data included in the technical literature, with commercial FEM software values and with measurements, showing very good agreement in all cases.

APPENDIX

TABLE III
PERMITTIVITY MEASUREMENTS OF TRANS-TECH MATERIALS
b=49.07 mm; $h_{\text{total}}=20$ mm; $h_d=0$ mm; $\sigma=0.955 \cdot 10^7$ S/m

Material dimensions	Meas. f_r [GHz]	Meas. Q	ϵ_r		
			Data sheet	This paper	NIST
D8623 a=29.83 mm h _m =3.36 mm	2.09567	2819	75	75.09-j.0.0020	79.6
D6 a=29.83 mm h _m =5.98 mm	2.03163	3510	6.3	6.54-j.0.0026	6.59

A. Values of $I_{mn}^{(s)}$ and $I_{mn}^{(c)}$ in (9)

Integrals $I_{mn}^{(s)}$ and $I_{mn}^{(c)}$ are:

$$I_{mn}^{(s)} = \int_{z=0}^h \cosh(\gamma_n z) \sin\left(2\pi m \frac{z}{h}\right) dz = \quad (25a)$$

$$= -\pi m h \operatorname{sinc}\left(\frac{n}{2} + m\right) \operatorname{sinc}\left(\frac{n}{2} - m\right)$$

$$I_{mn}^{(c)} = \int_{z=0}^h \cosh(\gamma_n z) \cos\left(2\pi m \frac{z}{h}\right) dz = \quad (25b)$$

$$= \frac{h}{2\chi_m} \delta(n - 2m)$$

and χ_n is defined as:

$$\chi_n = \begin{cases} 1/2 & , m = 0 \\ 1 & , m \neq 0 \end{cases} \quad (26)$$

B. Basis functions used in port 3

The basis functions used for the series expansion at port 3 (see magnetic field in port 3 in (14)) and port 4 are based on a generalization of the Dini series expansion [49] as reported in [50].

The general expression for the series expansion of a function $f(r)$ is:

$$f(r) = \sum_{m=0}^{\infty} \frac{c_m}{B(\mu_m)} \Phi_\nu(\mu_m r, \mu_m a), \quad a \leq r \leq b \quad (27)$$

where order ν is an arbitrary value and where the weights of the series expansion are:

$$c_m = \int_{r=a}^b r f(r) \Phi_\nu(\mu_m r, \mu_m a) dr \quad (28)$$

$$B(\mu_m) = \int_{r=a}^b r \Phi_\nu^2(\mu_m r, \mu_m a) dr$$

The basis function $\Phi_\nu(\mu_m r, \mu_m a)$ is:

$$\Phi_\nu(\mu_m r, \mu_m a) = \mu_m h_1 f_{1\nu}(\mu_m r, \mu_m a) - f_{2\nu}(\mu_m r, \mu_m a) \quad (29a)$$

$$f_{1\nu}(\mu_m r, \mu_m a) = \frac{\pi \mu_m a}{2} \cdot [Y_\nu'(\mu_m a) J_\nu(\mu_m r) - J_{-\nu}'(\mu_m a) \cdot Y_\nu(\mu_m r)] \quad (29b)$$

$$f_{2\nu}(\mu_m r, \mu_m a) = \frac{-\pi \mu_m a}{2} \cdot [Y_\nu(\mu_m a) J_\nu(\mu_m r) - J_{-\nu}'(\mu_m a) Y_\nu(\mu_m r)] \quad (29c)$$

Then, following these definitions, the series expansion in (27) is true if:

$$\begin{aligned} \Phi_v(\mu_m r, \mu_m a) + h_1 \left. \frac{\partial \Phi_v(\mu_m r, \mu_m a)}{\partial r} \right|_{r=a} &= 0 \\ \Phi_v(\mu_m r, \mu_m a) + h_2 \left. \frac{\partial \Phi_v(\mu_m r, \mu_m a)}{\partial r} \right|_{r=b} &= 0 \end{aligned} \quad (30)$$

The first equation is always true (and can be easily proved) and the second one implies that, for a given h_1 and h_2 :

$$\begin{aligned} \mu_m h_2 \left[\begin{array}{c} \mu_m h_1 f_{1v}'(\mu_m b, \mu_m a) \\ f_{2v}'(\mu_m b, \mu_m a) \end{array} \right] + \\ [\mu_m h_1 f_{1v}(\mu_m b, \mu_m a) - f_{2v}(\mu_m b, \mu_m a)] = 0 \end{aligned} \quad (31)$$

The zeros of this equation are the parameters μ_m used in the series expansion. In our case, we are using $v=1$ and $h_1=a$ and $h_2=b$, and then the basis function is:

$$\begin{aligned} \Phi_1(\mu_m r, \mu_m a) = \omega_{1m}(r) = \frac{\pi \mu_m^2 a^2}{2} \cdot \\ [J_1(\mu_m r) Y_0(\mu_m a) - J_0(\mu_m a) Y_1(\mu_m \cdot r)] \end{aligned} \quad (32)$$

where the function $\omega_{1m}(r)$ has been defined, and used in (14), and where μ_m are the zeros of:

$$\begin{aligned} \omega_{0m}(b) = \frac{\pi \mu_m^2 a^2}{2} \cdot \\ [J_0(\mu_m b) Y_0(\mu_m a) - J_0(\mu_m a) Y_0(\mu_m b)] = 0 \end{aligned} \quad (33)$$

It is important to remark that, apart from the trivial zero $\mu_0=0$, the rest of the zeros are the cut-off wave numbers of TM_{0m} modes in the coaxial waveguide.

Finally term $B(\mu_m)$, the normalization term in (28), is:

$$B(\mu_m) = \begin{cases} \frac{a^4 \mu_m^2}{2} \ln\left(\frac{b}{a}\right), & m = 0 \\ \frac{a^4 \mu_m^2}{2} \left[-1 + \left(\frac{J_0(\mu_m a)}{J_0(\mu_m b)} \right)^2 \right], & m > 0 \end{cases} \quad (34)$$

and it is important to note the zero in the origin ($\mu_m=0, m=0$), where function $\omega_{1m}(r)$ is:

$$\omega_{1m}(r) \Big|_{m=0} = \frac{a^2 \mu_m}{r} \quad (35)$$

where the coefficient $c_m, m=0$, in the series expansion is:

$$c_0 = a^2 \mu_m \int_{r=a}^b f(r) dr \quad (36)$$

Note that this case is the TEM mode.

C. Normalization term $N_q^{(e3)}$

$N_q^{(e3)}$ is a normalization term for the electric field [51, 52], and is calculated as:

$$\begin{aligned} \int_{r=a}^b h_q^{(3)}(r) h_m^{(3)}(r) r dr &= \\ = \int_{r=a}^b \omega_{1q}^{(3)}(r) N_q^{(e3)} \omega_{1m}^{(3)}(r) N_m^{(e3)} r dr &= \delta_{mq} \\ N_q^{(e3)} &= \begin{cases} \frac{1}{a^2 \mu_0 \sqrt{\ln(b/a)} \sqrt{2}}, & q = 0 \\ \frac{1}{a^2 \mu_q \sqrt{-1 + \left(\frac{J_0(\mu_m a)}{J_0(\mu_m b)} \right)^2}}, & q \neq 0 \end{cases} \end{aligned} \quad (37)$$

D. Value of integral $I_{qn}^{(\omega)}$ in (15)

Integral $I_{qn}^{(\omega)}$ is:

$$\begin{aligned} I_{qn}^{(\omega)} &= \int_{r=a}^b f'_{0n}(r) \cdot \omega_{1q}^{(3)}(r) \cdot r \cdot dr = \\ &= \begin{cases} \frac{-a \cdot k_{c0n}}{k_{c0n}^2 - k_{c0q}^2} \cdot f_{0n}(a) \cdot \omega_{1q}^{(3)}(a), & q > 0 \\ \frac{-a^2 \cdot f_{0n}(a)}{k_{c0n}}, & q = 0 \end{cases} \end{aligned} \quad (38)$$

ACKNOWLEDGMENT

The author Peñarada-Foix thanks to the Conselleria de Educaci3n of the Generalitat Valenciana for economic support to the stay in the U.S. (BEST/2010/210)

This work has been financed by the Ministry of Science and Innovation of Spain through the project MONIDIEL (TEC2008-04109)

REFERENCES

- [1] Juan A. Monsoriu, Miguel V. Andr3s, Anrique Silvestre, Albert Ferrando and Benito Gimeno, Analysis of Dielectric-Loaded Cavities Using an Orthonormal-Basis Method. *IEEE Trans. on Microwave Theory and Techniques*. vol. 50, no. 11, Nov. 2002, pp. 2545-2552.
- [2] S. Charmond, C. P. Carry, C. P. and D. Bouvard, Densification and microstructure evolution of Y-Tetragonal Zirconia Polycrystal powder during direct and hybrid microwave sintering in a single-mode cavity. *Journal of the European Ceramic Society*. vol. 30, no. 6, 2010, pp. 1211-1221 (doi:10.1016/j.jeurceramsoc.2009.11.014).
- [3] Thomas Baum, Lachlan Thompson and Kamran Ghorbani, Complex Dielectric Measurements of Forest Fire Ash at X-Band Frequencies. *IEEE Geoscience And Remote Sensing Letters*. vol. 8, no. 5, Sept. 2011, pp. 859-863.
- [4] Slawomir Hausman, Lukasz Januszkiewicz, Marina Michalak, Tomasz Kacprzak and Izabella Krucinska, High Frequency Dielectric Permittivity of Nonwoven. *FIBRES & TEXTILES in Eastern Europe*. vol. 14, no. 5, Jan./Dec. 2006, pp. 60-63.
- [5] Tomohiro Oguchi, Munehiro Udagawa, Noriyuki Nanba, Masayuki Maki and Yasuhiro Ishimine, Measurements of Dielectric Constant of Volcanic Ash Erupted From Five Volcanoes in Japan. *IEEE*

- Transactions On Geoscience And Remote Sensing*. vol. 47, no. 4, April 2009, pp. 1089-1096.
- [6] Raphaël Renoud, Caroline Borderon and Hartmut W. Gundel, Measurement and Modeling of Dielectric Properties of Pb(Zr,Ti)O₃ Ferroelectric Thin Films. *IEEE Transactions on Ultrasonics, Ferroelectrics and Frequency Control*. vol. 58, no. 9, Sept. 2011, pp. 1975-1980.
- [7] Mingwei Zhang, Jiwei Zhai and Xi Yao, Microwave dielectric properties of high dielectric tunable - low permittivity Ba_{0.5}Sr_{0.5}TiO₃-Mg₂(Ti_{0.95}Sn_{0.05})O₄ composite ceramics. *Ceramics International*. In Press, Corrected Proof, Available online 30 April 2011 (doi:10.1016/j.ceramint.2011.04.07).
- [8] C.C. Khaw, K.B. Tan and C.K. Lee, High temperature dielectric properties of cubic bismuth zinc tantalate. *Ceramics International*. vol. 35, no. 4, May 2009, pp. 1473-1480.
- [9] A. Chaouchi, S. d'Astorg and S. Marinel, Low sintering temperature of (Zn_{0.65}Mg_{0.35})TiO₃-xCaTiO₃-based dielectric with controlled temperature coefficient. *Ceramics International*. vol. 35, no. 5, July 2009, pp. 1985-1989.
- [10] Denis L. Guerra, Silze P. Oliveira, Ricardo A.S. Silva, Emiliano M. Silva and Adriano C. Batista, Dielectric properties of organofunctionalized kaolinite clay and application in adsorption mercury cation. *Ceramics International*. In Press, Corrected Proof, Available online 5 October 2011 (doi:10.1016/j.ceramint.2011.09.062).
- [11] Jerzy Krupka and Wociecz Gwarek, Measurements and Modeling of Planar Metal Film Patterns Deposited on Dielectric Substrates. *IEEE Microwave And Wireless Components Letters*. vol. 19, no. 3, March 2009, pp. 134-136.
- [12] Jerzy Krupka, Wojciech Gwarek, Norbert Kwietniewski and John G. Hartnett, Measurements of Planar Metal-Dielectric Structures Using Split-Post Dielectric Resonators. *IEEE Transactions On Microwave Theory And Techniques*. vol. 58, no. 12, Dec. 2010, pp. 3511-3518.
- [13] James Baker-Jarvis, Michael Janezic and Donald Degroot, High-frequency dielectric measurements. *IEEE Instrumentation Measurement Magazine*. vol. 13, no. 2, 2010, pp. 24-31.
- [14] Udo Kaatzte and Christof Hübner, Electromagnetic techniques for moisture content determination of materials. *Meas. Sci. Technol.* vol. 21, 2010, pp. 1-26. (doi:10.1088/0957-0233/21/8/082001)
- [15] Udo Kaatzte, Techniques for measuring the microwave dielectric properties of materials. *Metrologia*. vol. 47, 2010, pp. S91-S113.
- [16] Jerzy Krupka, Frequency domain complex permittivity measurements at microwave frequencies. *Meas. Sci. Tech.* vol. 17, 2006, pp. R55-R70.
- [17] J. Baker-Jarvis, M. D. Janezic, B. F. Riddle, R. T. Johnk, P. Kabos, C. L. Holloway, R. G. Geyer and C. A. Grosvenor, Measuring the permittivity and permeability of lossy materials: solids, liquids, metals, building materials and negative index materials. NIST Technical Note 1536, Feb. 2005.
- [18] Felipe L. Penaranda-Foix, Pedro J. Plaza-González, Beatriz García-Baños and Daniel Polo-Nieves, "A Non-destructive Method of Measuring the Dielectric and Magnetic Properties of Laminate Materials in Open Cavities". *Proc. Of the IMS2004*, Fort Worth, TX (USA) 2004, vol. 3, pp. 1821-1823.
- [19] Michael D. Janezic and James Baker-Jarvis, "Full-Wave Analysis of a Split-Cylinder Resonator for Nondestructive Permittivity Measurements". *IEEE Trans. Microwave Theory and Tech.*, vol. 47, No. 10, Oct. 1999, pp. 2014-2020.
- [20] James Baker-Jarvis, Michael D. Janezic, Paul D. Domich and Richard G. Geyer, Analysis of an Open-Ended Coaxial Probe with Lift-Off for Nondestructive Testing, *IEEE Trans. On Instrumentation and Measurement*, vol. 43 No 5, Oct. 1994, pp. 711-718.
- [21] A. Taflove, "Computational Electrodynamics: the Finite-Difference Time-Domain Method". Norwood, MA: Artech House, 1995.
- [22] J. Volakis, "Finite Element Method for Electromagnetics", New York: IEEE Press, 1998.
- [23] Alvin Wexler, Solution of Waveguide Discontinuities by Modal Analysis. *IEEE Transactions On Microwave Theory And Techniques*. vol. 15, no. 9, Sept. 1967, pp. 508-517.
- [24] H. Patzelt and F. Arndt, Double-Plane Steps in Rectangular Waveguides and their Application for Transformers, Irises, and Filters. *IEEE Transactions On Microwave Theory And Techniques*. vol. 30, no. 5, May 1982, pp. 771-776.
- [25] G. Conciauro, M. Guglielmi and R. Sorrentino, "Advanced Modal Analysis". New York: Wiley, 2000.
- [26] J.A. Ruiz-Cruz, J. Esteban and J.M. Rebolgar, Efficient boundary contour mode-matching method of H- and E-plane junctions by fast Fourier transform algorithm. *IEE Proc. Microw. Antenas Propag.*, vol. 150, No. 5, October 2003, pp. 332-338.
- [27] J. Gil, A.A. San Blas, C. Vicente, B. Gimeno, M. Bressan, V.E. Boria, G. Conciauro and M. Maestre, Full-Wave Analysis and Design of Dielectric-Loaded Waveguide Filters Using a State-Space Integral-Equation Method. *IEEE Transactions on Microwave Theory and Techniques*, vol. 57, No. 1, Jan. 2009, pp. 109-120.
- [28] J. Gil, A.M. Perez, B. Gimeno, M. Bressan, V.E. Boria and G. Conciauro, Analysis of Cylindrical Dielectric Resonators in Rectangular Cavities Using a State-Space Integral-Equation Method. *IEEE Microwave and Wireless Components Letters*, vol. 16, No. 12, Dec. 2006, pp. 636-638.
- [29] James Baker-Jarvis and Bill F. Riddle, Dielectric Measurements Using a Reentrant Cavity: Mode-Matching Analysis. NIST Technical Note 1384, Nov. 1996.
- [30] R. Lech and L. Mazur, Analysis of Circular Cavity With Cylindrical Objects. *IEEE Transactions On Microwave Theory And Techniques*. vol. 55, no. 10, Oct. 2007, pp. 2115-2123.
- [31] Weiguo Xi and Wayne R. Tinga, Field Analysis of New Coaxial Dielectric Resonator. *IEEE Trans. on Microwave Theory and Techniques*. vol. 40, no. 10, Oct. 1992, pp. 1927-1934.
- [32] Jingliang Zheng and Ming Yu, Rigorous Mode-Matching Method of Circular to Off-Center Rectangular Side-Coupled Waveguide Junctions for Filter Applications. *IEEE Trans. on Microwave Theory and Techniques*. vol. 55, no. 11, Nov. 2007, pp. 2365-2373.
- [33] Felipe L. Penaranda-Foix, "Application of the Generalized Circuit Analysis Theory to the Resolution of Electromagnetic Diffraction Problems" (in Spanish), Ph.D. dissertation, Universidad Politécnica de Valencia, Valencia, Spain, 2001.
- [34] Felipe L. Penaranda-Foix and Miguel Ferrando-Bataller, "Scattering of Inhomogeneous Cylinders by Circuit Analysis". *Microwave and Optical Technology Letters*, Vol 39, N. 2, Oct. 2003, pp. 155-159.
- [35] Felipe L. Penaranda-Foix, Jose M. Catala-Civera, Antoni J. Canos-Marin and Pedro J. Plaza-Gonzalez, "Solving Cylindrically-Shaped Waveguides Partially-Filled with Isotropic Materials by Modal Techniques", in *Proc. of 11th. AMPERE 2007*, Oradea (Romania), 2007, vol. 1, pp. 67-70.
- [36] P. Arcioni, M. Bozzi, M. Bressan, G. Conciauro and L. Perreggini, Frequency/time-domain modelling of 3D waveguide structures by a BI-RME approach. *International Journal of Numerical Modelling: Electronic Networks, Devices and Fields*. *International Journal of Numerical Modelling: Electronic networks, Devices and Fields*. vol. 15, no. 1, 2002, pp. 3-21.
- [37] P. Soto, V. E. Boria, J. M. Catalá-Civera, N. Chouaib, N., M. Guglielmi and B. Gimeno, Analysis, Design, and Experimental Verification of Microwave Filters for Safety Issues in Open-Ended Waveguide Systems. *IEEE Transactions On Microwave Theory And Techniques*. vol. 48, no. 11, Nov. 2000, pp. 2133-2140.
- [38] T. Sieverding and F. Arndt, Field theoretical cad of open or aperture matched T-junction coupled rectangular waveguide structures. *IEEE Transactions On Microwave Theory And Techniques*. vol. 40, no. 2, Feb. 1992, pp. 353-362.
- [39] J. M. Rebolgar, J. Esteban and J. E. Page, Fullwave analysis of three and port-port rectangular waveguide junctions. *IEEE Transactions On Microwave Theory And Techniques*. vol. 42, no. 2, Feb. 1994, pp. 256-263.
- [40] M. Ludovico, B. Piovano, G. Bertin, C. Zarba, L. Accatino and M. Mongiardo, CAD and optimization of compact ortho-mode transducers. *IEEE Transactions On Microwave Theory And Techniques*. vol. 47, no. 12, Dec. 1999, pp. 2479-2486.
- [41] A. Alvarez, G. Connor and M. Guglielmi, New simple procedure for the computation of the multimode admittance or impedance matrix of planar waveguide junctions. *IEEE Transactions On Microwave Theory And Techniques*. vol. 44, no. 3, March 1996, pp. 413-418.
- [42] H. Kawabata, H. Tanpo and Y. Kobayashi, Analysis and Experiments of a TM₀₁₀ Mode Cylindrical Cavity to Measure Accurate Complex Permittivity of Liquid. *IEICE Trans. Electron.* vol. E87-C, no. 5, May 2004, pp. 694-699.
- [43] Hirokazu Kawabata, Yoshio Kobayashi and Syougo Kaneko, Analysis of Cylindrical Cavities to Measure Accurate Relative Permittivity and

- Permeability of Rod Samples. *Proceedings of Asia-Pacific Microwave Conference 2010*, pp. 1459-1462.
- [44] Felipe L. Penaranda-Foix and Jose M. Catala-Civera, "Circuitual analysis of cylindrical structures applied to the electromagnetic resolution of resonant cavities", Chapter 7 in *Passive Microwave Components and Antennas*, 1st ed, Ed. IN-TECH, April 2010 (ISBN 978-953-307-083-4). Hardcopy and Online paper are available at webpage: <http://sciendo.com/books/show/title/passive-microwave-components-and-antennas>.
- [45] J.M. Rebellar and J.A. Encinar, Field Theory Analysis of Multiport-Multidiscontinuity Structures: An application to Short-circuited E-plane Septum. *IEE Proc. Part H, Microw. Antenas Propag.*, vol. 135, Pt. H, No. 1, February 1988, pp. 1-7.
- [46] J. D. Wade and R. H. MacPhie, Conservation of complex power technique for waveguide junctions with finite wall conductivity. *IEEE Trans. on Microwave Theory and Techniques*, vol. 35, No. 4, April 1990, pp. 373-378.
- [47] Jerzy Krupka and Janina Mazierska, Contactless Measurements of Resistivity of Semiconductor Wafers Employing Single-Post and Split-Post Dielectric-Resonator Techniques. *IEEE Trans. on Instrumentation and Measurements*, vol. 56, no. 5, Oct. 2007, pp. 1839-1844.
- [48] C. A. Balanis, "Advanced Engineering Electromagnetics". John Wiley & Sons, 1989.
- [49] G. N. Watson, "A Treatise on the Theory of Bessel Functions". Cambridge Mathematical Library, 1995.
- [50] B. G. Korenev, "Bessel Functions and their Applications". Taylor and Francis, 2002.
- [51] G. G. Gentili, Properties of TE-TM mode-matching techniques. *IEEE Trans. on Microwave Theory and Techniques*, vol. 39, no. 9, Sept. 1991, pp. 1669-1673.
- [52] G. V. Eleftheriades, A. S. Omar and L. P. B. Katehi, Some Important Properties of Waveguide Junction Generalized Scattering Matrices in the Context of the Mode Matching Technique. *IEEE Trans. on Microwave Theory and Techniques*, vol. 42, no. 10, Oct. 1994, pp. 1896-1903.
- [53] Robert E. Collin, "Foundations for Microwave Engineering". IEEE Press Classic Reissue, 2001.
- [54] M. A. Leontovich, On the approximate boundary conditions for electromagnetic fields on the surface of well conducting bodies. *Investigations of Propagation of Radio Waves*, vol. B. A. Vvdensky, Ed. Moscow: Academy of Sciences USSR, pp. 5-20, 1948.
- [55] T. B. Senior, Impedance boundary conditions for imperfectly conducting surfaces. *Applied Science Research*, vol. 8, pp. 418-436, 1960.
- [56] R. F. Harrington, "Time-Harmonic Electromagnetic Fields", McGraw Hill, New York, 1961.
- [57] Felipe L. Penaranda-Foix, Jose M. Catala-Civera, Antoni J. Canos-Marin and Beatriz Garcia-Banos, "Circuitual analysis of a coaxial re-entrant cavity for performing dielectric measurement", in *Proc. of the IMS2009*, Boston, MA (USA) 2009, vol. 1 pp. 1309-1312.
- [58] Weiguo Xi, Wayne R. Tinga, W. A. Geoffrey Voss and Bai Quiang Tian, New Results for Coaxial Re-Entrant Cavity with Partially Filled Gap. *IEEE Trans. on Microwave Theory and Techniques*, vol. 40, no. 4, April 1992, pp. 747-753.
- [59] Marek Jaworski, On the Resonant Frequency of a Re-entrant Cylindrical Cavity. *IEEE Trans. on Microwave Theory and Techniques*, vol. 26, no. 4, April 1978, pp. 256-260.
- [60] A. G. Williamson, The resonant frequency and tuning characteristics of a narrow-gap Re-entrant Cavity. *IEEE Trans. on Microwave Theory and Techniques*, vol. 24, no. 4, April 1976, pp. 182-187.
- [61] Richard G. Carter, Jinjun Feng and Ulrich Becker, Calculation of the Properties of Reentrant Cylindrical Cavity Resonators. *IEEE Trans. On Microwave Theory and Techniques*, vol. 55, No. 12, Dec. 2007, pp. 2531-2538.
- [62] Hyo J. Eom, Young C. Noh and Jong K. Park, Scattering Analysis of a Coaxial Line Terminated by a Gap. *IEEE Microwave and Guided Wave Letters*, Vol. 8, No. 6, June 1998, pp. 218-219.
- [63] Andrew R. Weily and Ananda S. Mohan, Rotationally Symmetric FDTD for Wideband Performance Prediction of TM₀₁ DR Filters. *International Journal of RF and Microwave Computer-Aided Engineering*, vol. 12, no. 3, 2002, pp. 259-271.
- [64] Chi Wang, Kawthar A. Zaki, Ali E. Atia and Tim G. Dolan, Dielectric Compline Resonators and Filters. *IEEE Trans. on Microwave Theory and Techniques*, vol. 46, no. 12, Dec. 1998, pp. 2501-2506.
- [65] Kawthar A. Zaki and Chunming Chen, New Results in Dielectric-Loaded Resonators. *IEEE Trans. on Microwave Theory and Techniques*, vol. 34, no. 7, July 1986, pp. 815-824.
- [66] Jeffrey C. Lagarias, James A. Reeds, Margaret H. Wright and Paul E. Wright, *Convergence Properties of the Nelder-Mead Simplex Method in Low Dimensions*. *SIAM Journal of Optimization*, 9(1), 1998, p.112-147.
- [67] A. J. Canos, J. M. Catala-Civera, F. L. Penaranda-Foix and E. Reyes-Davo, A novel technique for deembedding the unloaded resonance frequency from measurements of microwave cavities. *IEEE Transactions on Microwave Theory and Techniques*, vol. 54, no. 8, Aug. 2006, pp. 3407-3416.